On the crystal structures and phase transitions of hydrates in the binary system, dimethyl sulfoxide (DMSO) – water.

Supplementary Figures and Tables

A. D. Fortes,[1] J. Ponsonby,[1,2] O. Kirichek,[1] V. García-Sakai[1]

[1]ISIS Pulsed Neutron and Muon Source, Rutherford Appleton Laboratory, Harwell Science and Innovation Campus, Chilton, Oxfordshire OX11 0QX

[2]Faculty of Science, University of Bath, Claverton Down, Bath, Somerset BA2 7AY, United Kingdom.

Corresponding author email: dominic.fortes@stfc.ac.uk

Supplementary Figures

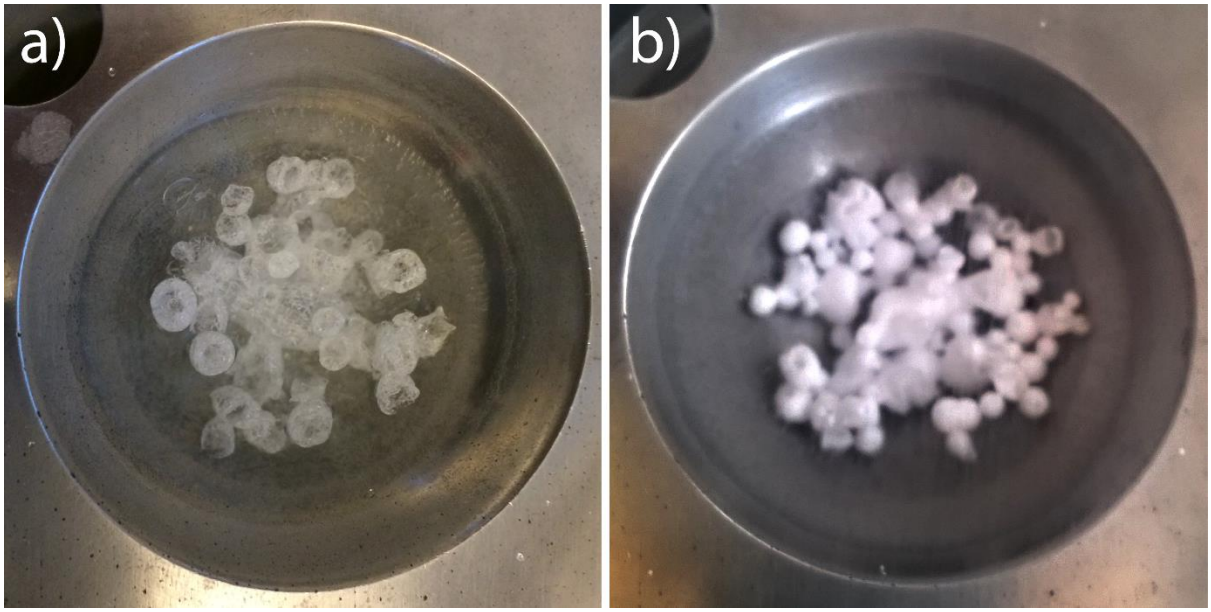

Figure S1

Photographs of sample-1 (left) and sample-5 (right) immediately after freezing of the aqueous solution droplets in liquid nitrogen. Notice that the spherules in sample-1 are transparent and slightly larger (3.5 – 5.5 mm) than the opaque sample-5 spherules (2.0 – 5.0 mm). The steel cryomortar holding the samples has a bowl diameter of 65.5 mm, a depth of 21 mm, and volume of 40.2 cm^3.

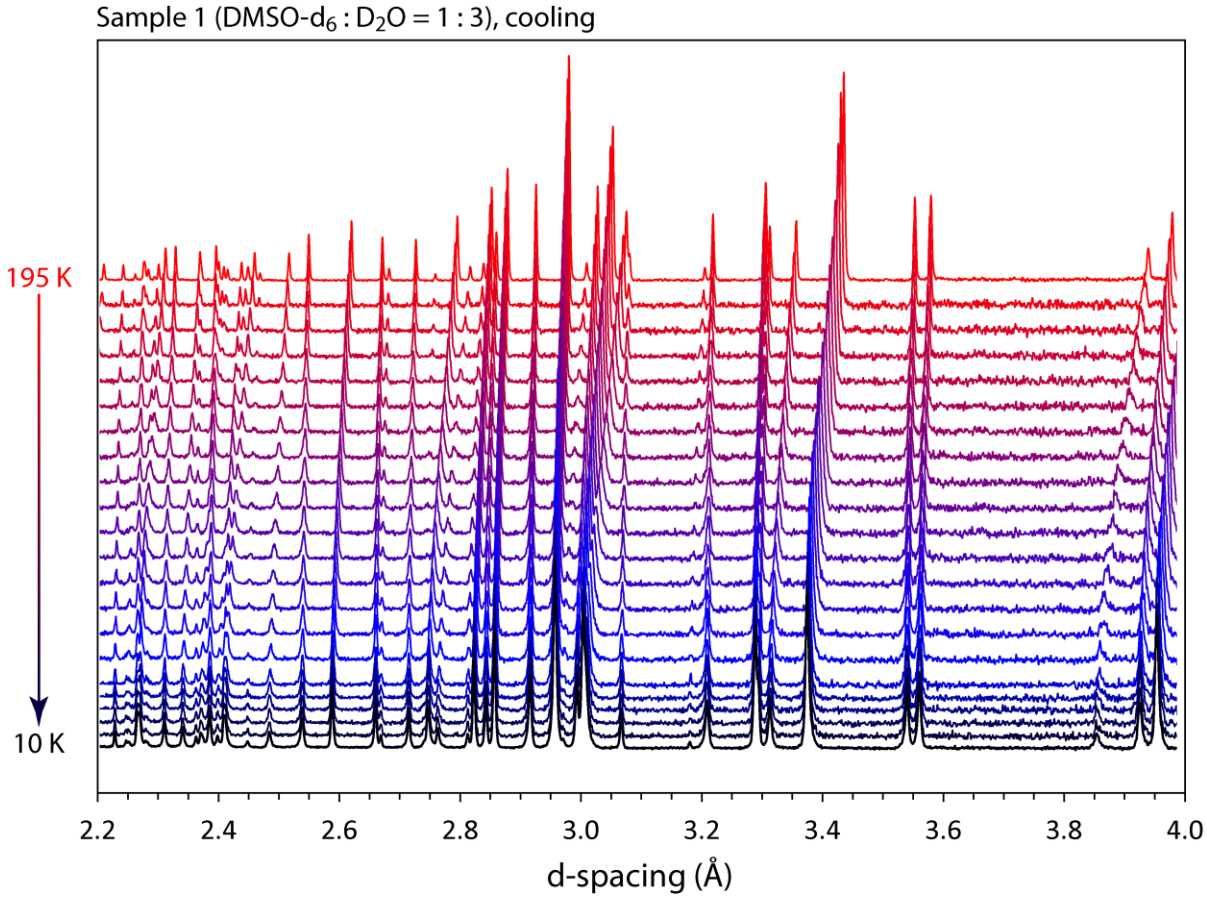

Figure S2a

Stackplot of neutron powder diffraction data collected from sample-1 (phase pure DMSO trihydrate) on cooling from 195 K (top) to 10 K (bottom). As expected, peaks shift to shorter d-spacings due to contraction of the unit cell on cooling, but the shifts are not uniform by virtue of the crystal's anisotropy.

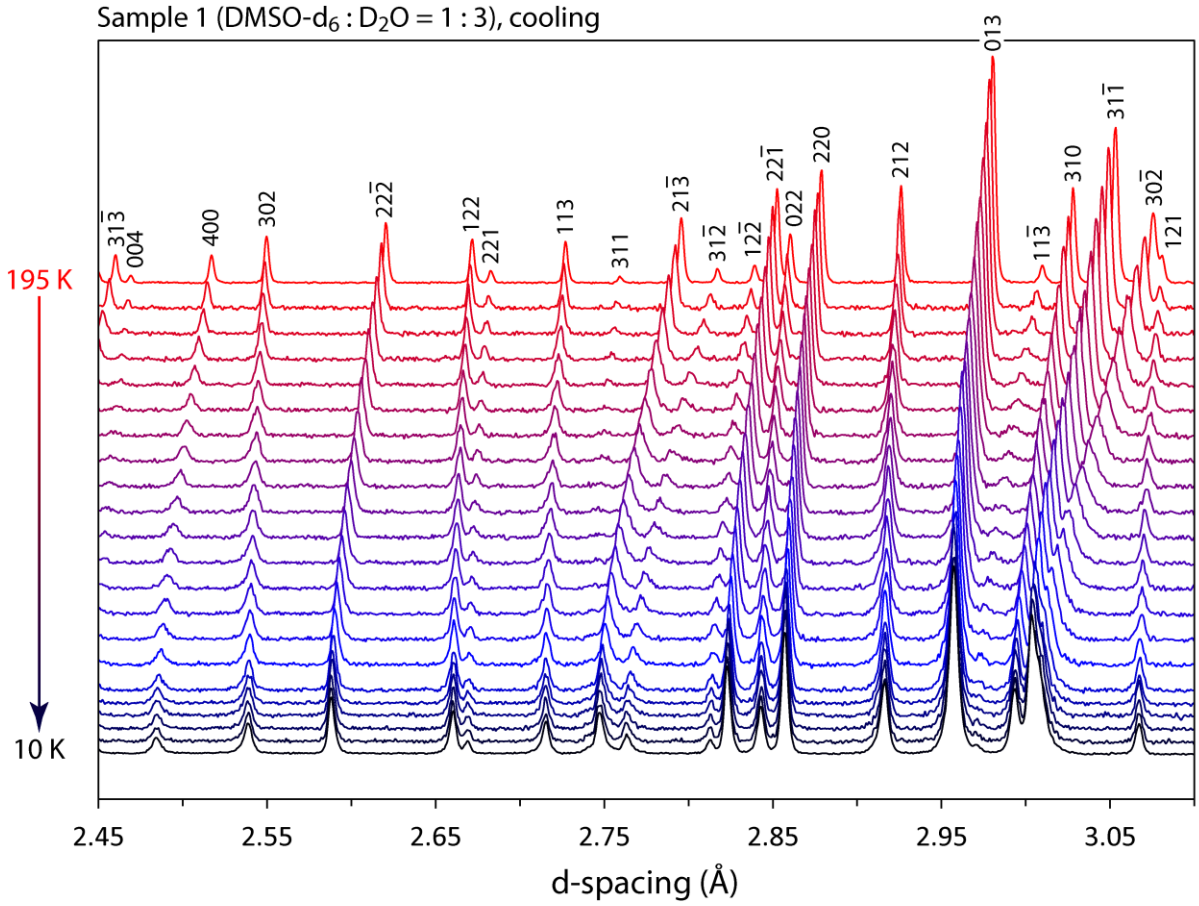

Figure S2b

An expanded view of Figure S2a with the diffraction indices of each Bragg peak marked. This gives a clearer illustration of the peak broadening that occurs on cooling.

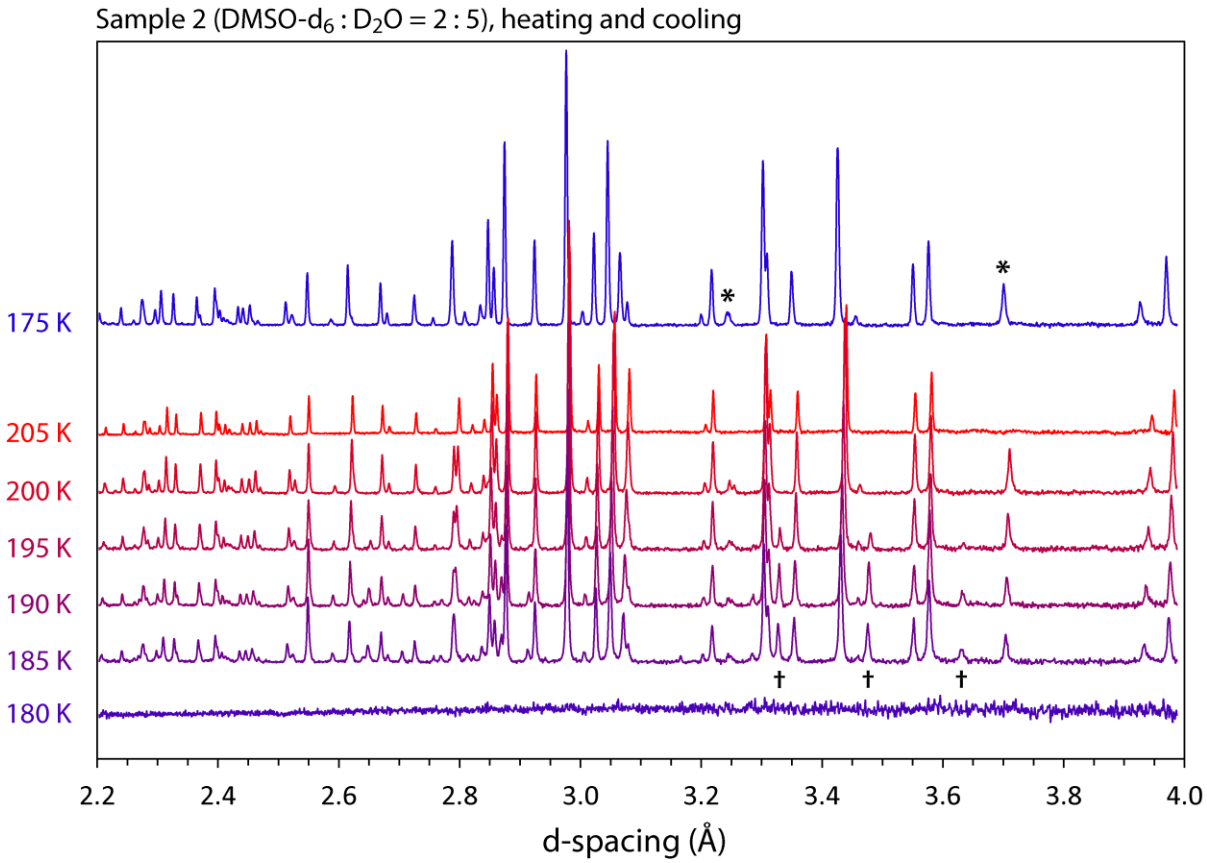

Figure S3

Stackplot of neutron powder diffraction data collected from sample-2, starting from the amorphous phase (exhibiting no Bragg peaks) at 180 K, followed by crystallisation and a series of phase transitions on warming to 205 K. The uppermost diffraction pattern was acquired after cooling back to 175 K. Asterisks mark the strongest peaks from anhydrous DMSO, which disappear at 205 K due to partial melting, and reappear at 175 K by freezing of the partial melt. The dagger symbols mark the strongest Bragg peaks from α-DMSO dihydrate.

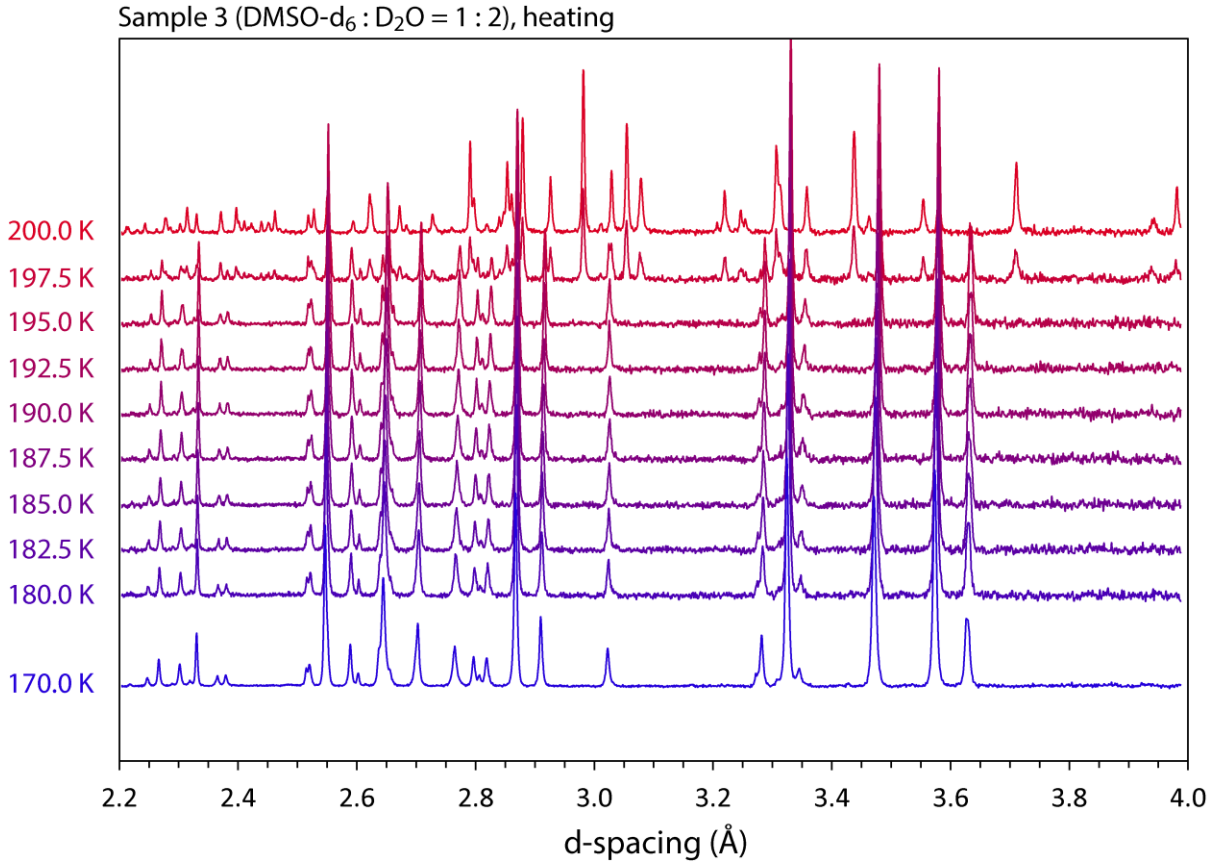

Figure S4

Stackplot of neutron powder diffraction data collected from sample-3, which – after crystallisation – consists of phase-pure α-DMSO dihydrate. An abrupt phase transition to a mixture of DMSO and DMSO trihydrate is evident from the change in the diffraction pattern at 197.5 and 200 K.

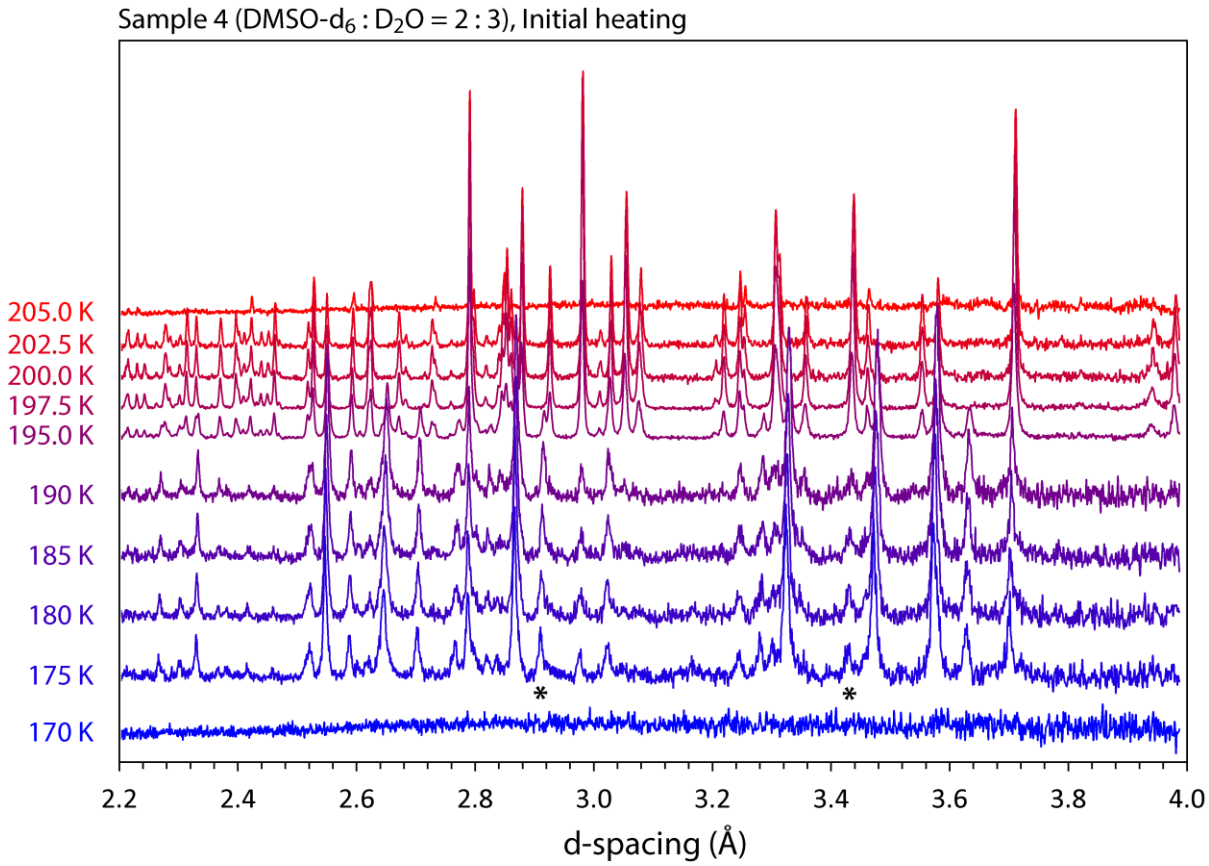

Figure S5

Stackplot of neutron powder diffraction data collected from sample-4 during its first heating cycle. The initially amorphous phase at 170 K transforms on heating to a mixture of crystalline DMSO, α-DMSO dihydrate and some DMSO trihydrate (peaks marked with asterisks). Between 190 and 195 K, the dihydrate phase transforms completely to trihydrate + DMSO, and then undergoes partial melting to DMSO + liquid between 202.5 and 205 K.

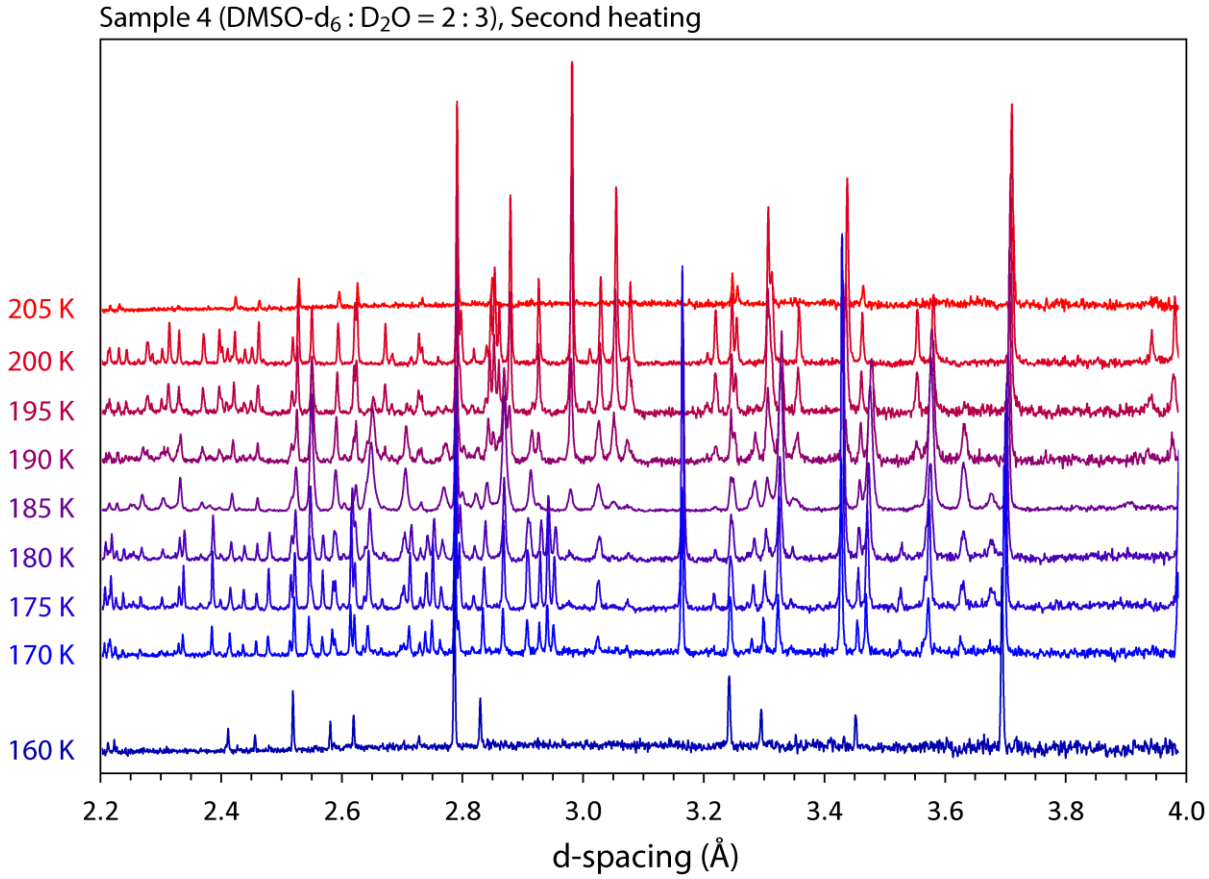

Figure S6

Stackplot of neutron powder diffraction data collected from sample-4 during its second heating cycle. The sample shown at 205 K in Figure S5 was rapidly cooled to 100 K; subsequent warming to 160 K (bottom trace here) shows it to contain only crystalline DMSO as well as an amorphous residue. At 170 K, the amorphous residue crystallises into β-DMSO dihydrate with some α-dihydrate. The beta phase persists up to 180 K; the remaining α-dihydrate once again breaks down to DMSO + DMSO trihydrate between 190 and 195 K.

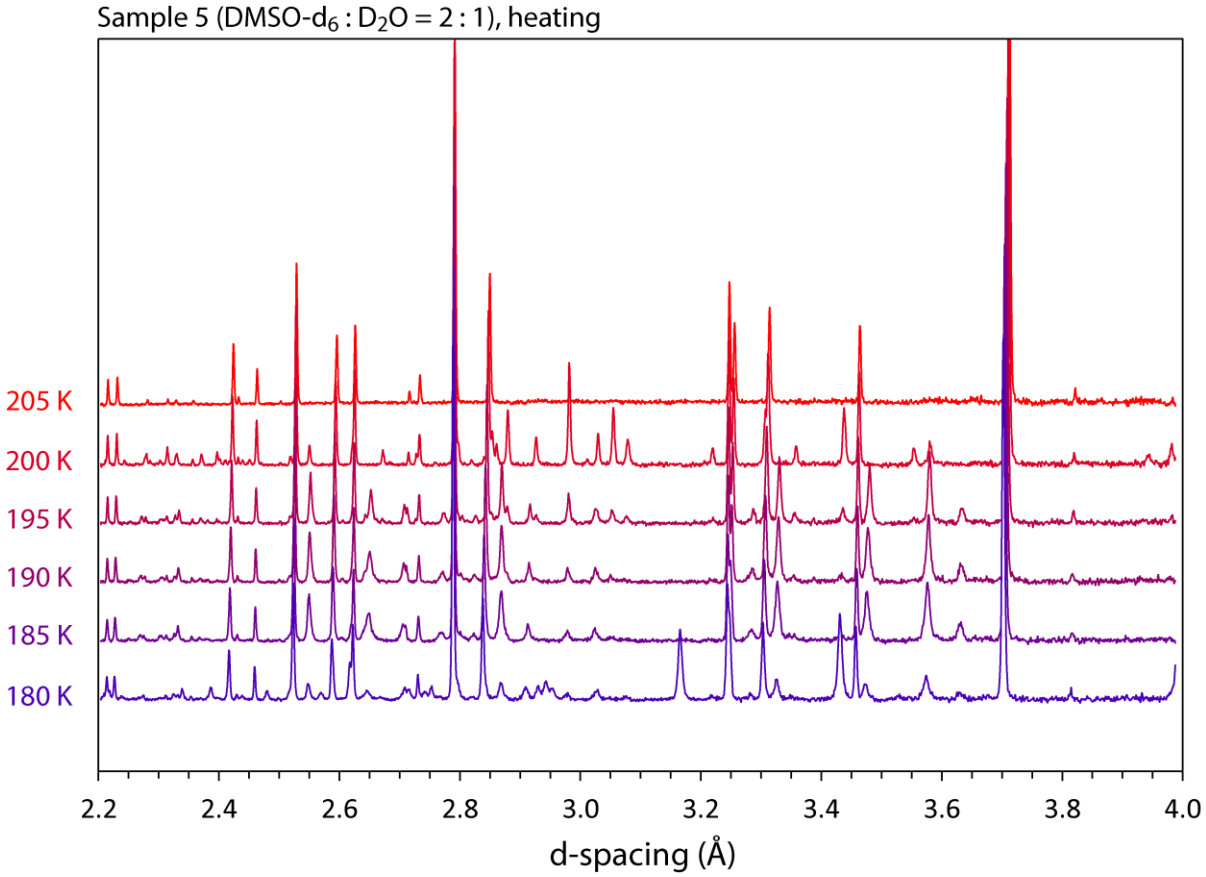

Figure S7

Stackplot of neutron powder diffraction data collected from sample-5. This specimen was already partially crystalline at 100 K, containing DMSO + glass. Warming to 180 K resulted in the amorphous component crystallising into a mixture of α- and β-DMSO dihydrate. The β-dihydrate was absent on warming to 185 K, and the remaining α-dihydrate underwent a reaction to DMSO + DMSO trihydrate during further warming, which was complete by 200 K. At 205 K, we observed a partially molten mixture of DMSO + liquid.

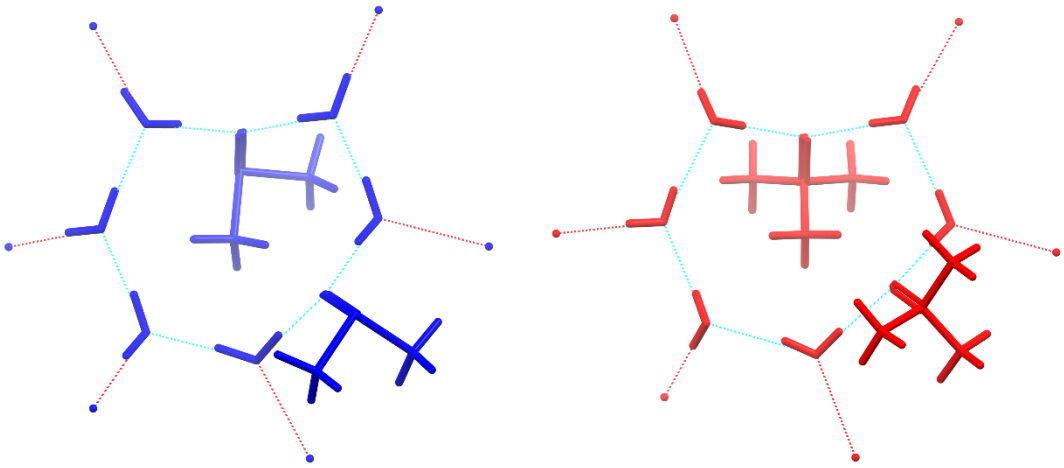

Figure S8

Schematic illustration of the $R_8^6(16)$ rings in α-DMSO dihydrate (left, in blue) and in trimethylamine N-oxide (TMAO) dihydrate (right, in red). Molecules are drawn as solid rods; dashed turquoise lines depict the hydrogen bonds in the ring, and red dashed lines show the H-bonds forming partial adjacent rings. The DMSO and TMAO molecules are shown in the 12 o'clock position (pointed inwards and below the ring plane) and the 4 o'clock position (projected outwards and above the ring plane). The scale of both illustrations is identical.

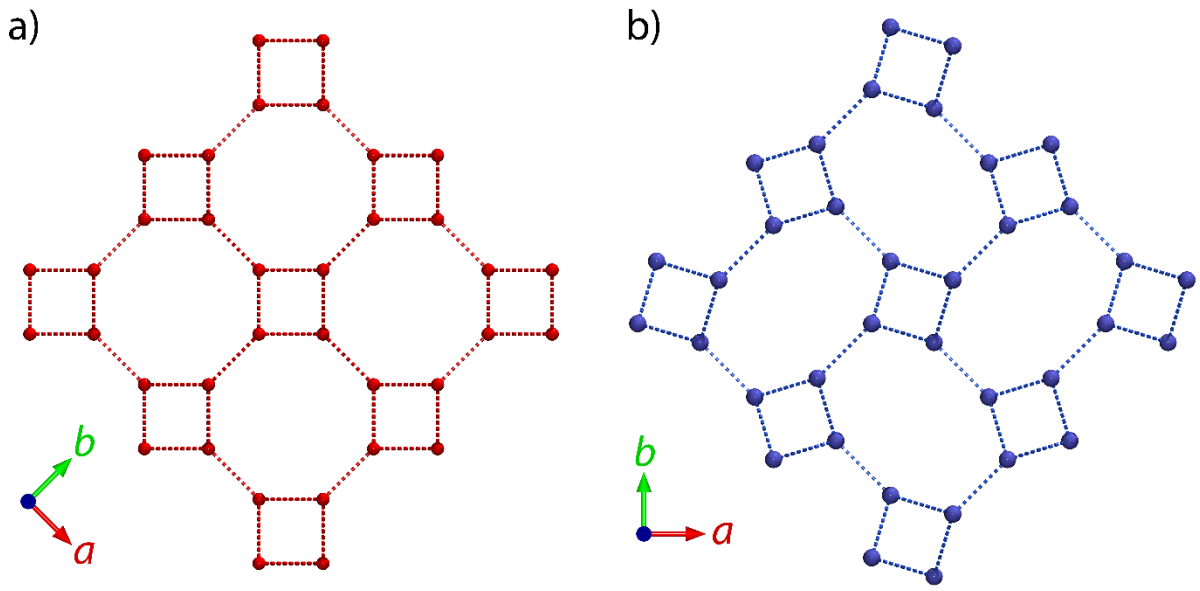

Figure S9

Nodal connectivity of the sheets from one of the two interpenetrating frameworks in ice VI (left) and the framework of edingtonite (right), showing a similar geometric arrangement of 4-sided and 8-sided rings to that found in the water–water sheets of DMSO trihydrate.

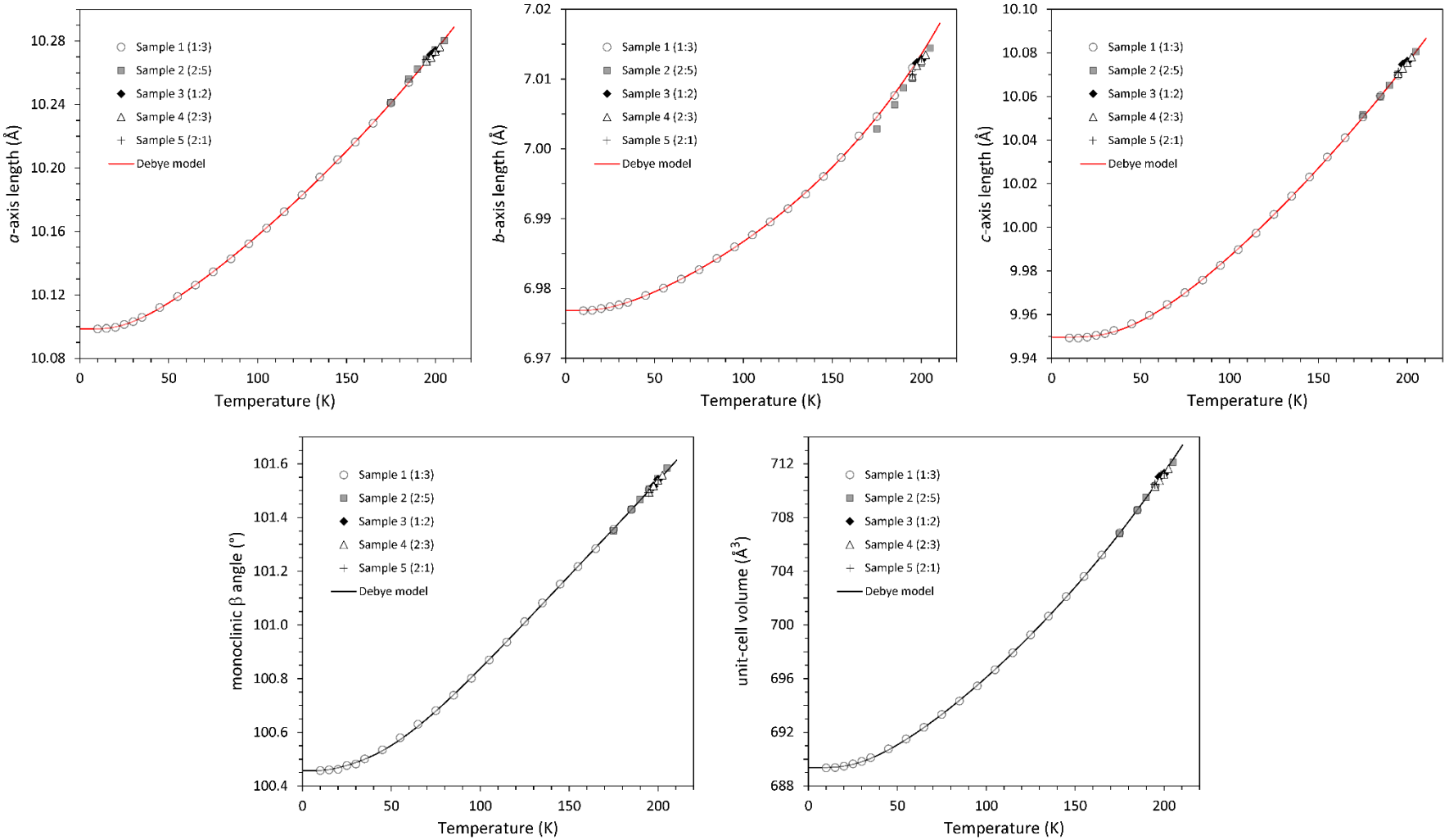

Figure S10

Plots of the unit-cell parameters of DMSO-d_6·3D_2O using the data reported in Table S2 below. Points between 10 and 195 K from Sample-1 were used to fit the solid lines using a 2nd-order Debye model (*cf.*, Table S3). Error bars are smaller than the symbols.

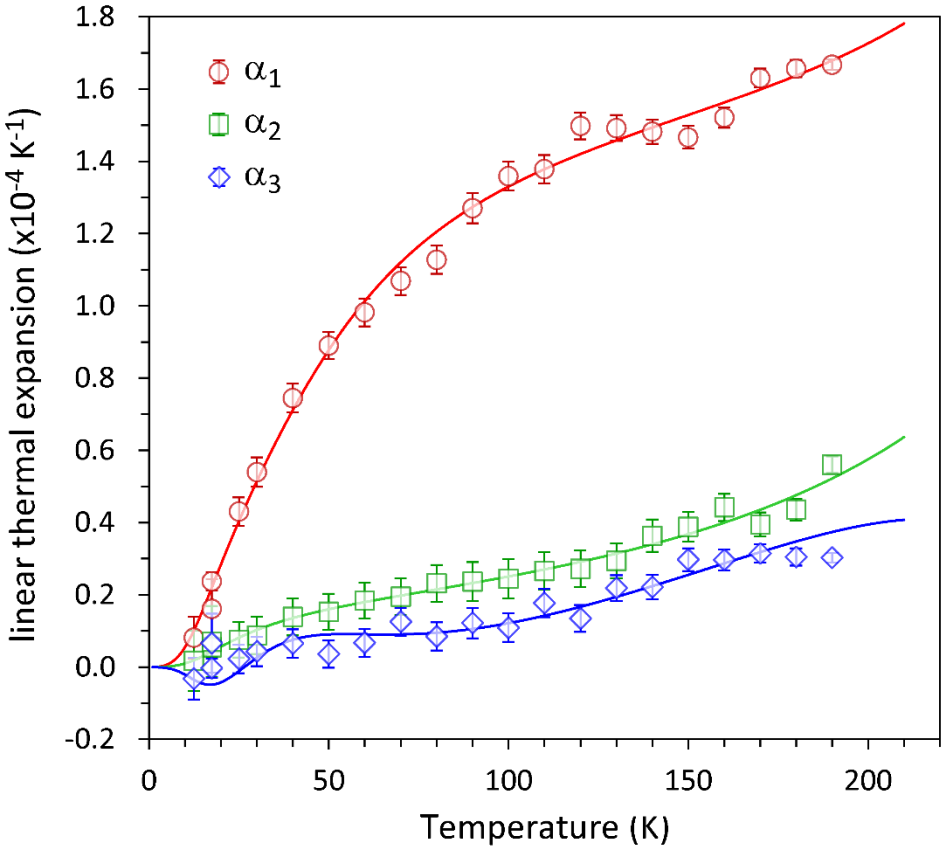

Figure S11

Magnitudes of the principal directions of the thermal expansion tensor for DMSO-d_6·3D_2O as a function of temperature. The direction α_2 is fixed by symmetry along the 2-fold axis of the crystal; the orientation of α_1 and α_3 is shown in the main text, Figure 19. Points are obtained from the refined lattice parameters (Sample-1, 10–195 K) and the solid lines from the fitted 2nd-order Debye model.

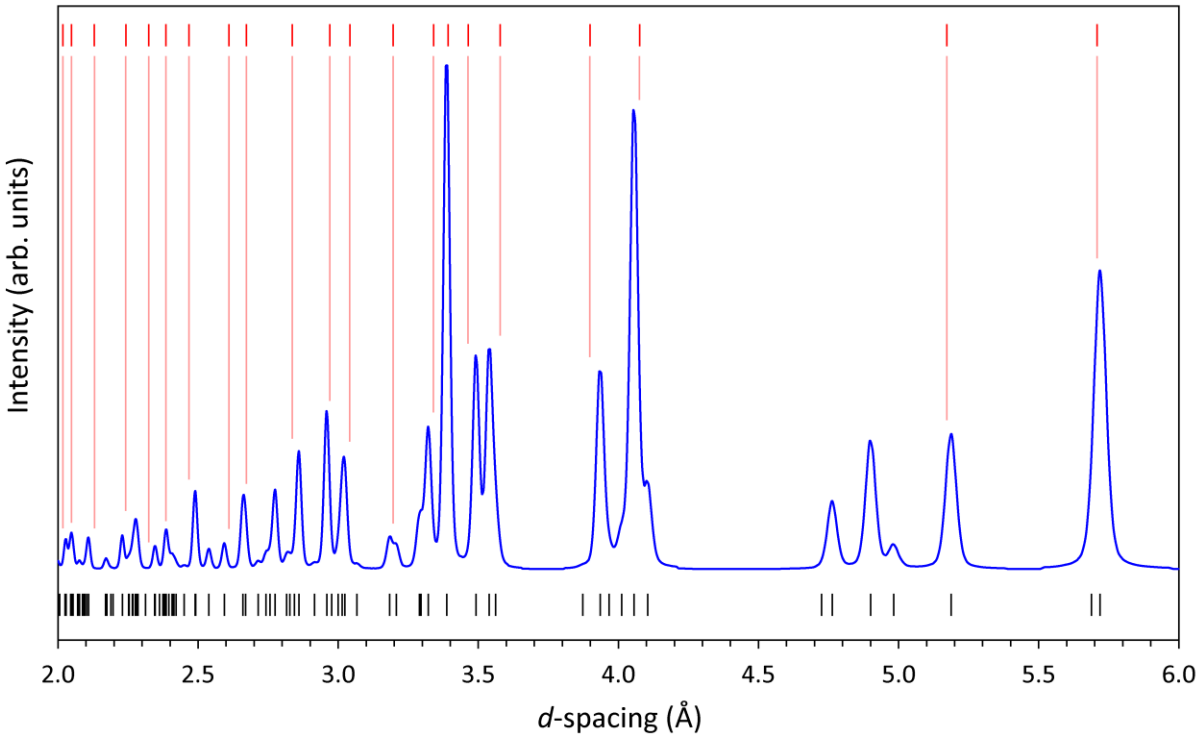

Figure S12

Simulated X-ray powder diffraction pattern of DMSO trihydrate (blue line) between 2.0 – 6.0 Å *d*-spacing. Reflection positions are marked by the black vertical lines underneath the profile. The red tick marks and pale descending lines above the diffraction pattern show the peak positions tabulated by Boutron & Kaufmann (1978) for their unknown hydrate, observed in flash-frozen 45 wt. % DMSO solution between 77 and 93 K, *after we have subjected the values to a zero shift of −0.4°*. Note that we have also deliberately broadened the peaks of the simulated pattern to match what we believe the resolution of their system may have been.

There is a reasonably convincing degree of agreement between the simulation and the observed peaks of Boutron & Kaufmann (1978). Some quite strong peaks are 'missing', particularly between 4.7 – 5.0 Å and at 10.05 Å (not shown), which are not readily explained. Their experimental setup produced parasitic Bragg peaks from Mylar and beryllium, but these should not mask any intensity from the sample in this region. Equally, the beam-stop evident in Figure 1 of Boutron and Kaufmann's paper only has an angular radius of ~ 5°, so cannot account for the missing 10 Å peak.

Nevertheless, we note that the tabulated peaks for ice I*h* in their paper are missing some peaks and are extremely inaccurate, even allowing for a large zero shift, so the degree of agreement we see for the DMSO trihydrate peaks is actually quite good.

Supplementary Tables

Table S1

Refined phase fractions (wt. %) of the phases present in each sample as a function of temperature. Where these could not be determined – because the sample was partially amorphous, or contained a phase with an unknown structure – the table simply notes the presence of phases with a tick.

Sample-1

T (K)	Amorphous	$DMSO{\cdot}3D_2O$	α-$DMSO{\cdot}2D_2O$	DMSO
195	0	100	0	0
≤ 185	100 (solid)	0	0	0

Sample-2

T (K)	Amorphous	$DMSO{\cdot}3D_2O$	α-$DMSO{\cdot}2D_2O$	DMSO
205	Liquid	✓	0	0
200	0	90.2	0.0	9.8(2)
195	0	87.2	5.0(1)	7.8(1)
190	0	79.8	13.9(3)	6.3(2)
185	0	79.3	14.6(3)	6.1(2)
≤ 180	100 (solid)	0	0	0

Sample-3

T (K)	Amorphous	$DMSO{\cdot}3D_2O$	α-$DMSO{\cdot}2D_2O$	DMSO
200.0	0	80.1	0	19.9(3)
197.5	0	35.6	56.0(3)	8.4(2)
175 – 195	0	0	100	0
≤ 170	100 (solid)	0	0	0

Sample-4

T (K)	Amorphous	$DMSO{\cdot}3D_2O$	α-$DMSO{\cdot}2D_2O$	DMSO
205.0	Liquid	0	0	✓
202.5	0	67.0	0	33.0(3)
200.0	0	69.5	0	30.5(2)
197.5	0	69.4	0	30.6(2)
195	0	44.6	30.9(3)	24.5(2)
190	0	9.7	75(1)	15.3(7)
185	0	9.5	76(1)	14.4(7)
180	0	9.1	77(1)	13.9(7)
175	0	9.0	77(1)	14.0(8)
≤ 170	100 (solid)	0	0	0

Table S1, continued

Sample-5

T (K)	Amorphous	$DMSO \cdot 3D_2O$	α-$DMSO \cdot 2D_2O$	DMSO
205	Liquid	0	0	✓
200	0	30.2	0	69.8(3)
195	0	10.4	25.0(3)	64.6(4)
190	0	5.7	29.3(8)	64.9(9)
185	0	5	30(1)	65(1)
180	0	0	$\alpha + \beta$	✓
≤ 170	Solid	0	0	✓

Table S2

Refined lattice parameters of DMSO-d_6·3D_2O as a function of temperature from each of the samples in which the phase occurred.

T (K)	*a* (Å)	*b* (Å)	*c* (Å)	β (°)	V (Å^3)
Sample-1					
195	10.26711(4)	7.01160(3)	10.06980(4)	101.5042(3)	710.351(3)
185	10.25391(8)	7.00768(6)	10.06027(7)	101.430(1)	708.556(6)
175	10.24097(9)	7.00462(6)	10.05061(9)	101.356(1)	706.856(7)
165	10.22819(10)	7.00186(7)	10.04107(10)	101.284(1)	705.204(8)
155	10.21627(12)	6.99876(8)	10.03219(11)	101.217(1)	703.612(9)
145	10.20524(13)	6.99604(8)	10.02308(13)	101.152(1)	702.098(10)
135	10.19430(14)	6.99350(8)	10.01434(14)	101.082(1)	700.648(10)
125	10.18299(15)	6.99144(9)	10.00594(15)	101.012(1)	699.245(11)
115	10.17241(16)	6.98954(9)	9.99742(15)	100.936(1)	697.914(11)
105	10.16206(16)	6.98768(9)	9.98983(16)	100.870(1)	696.643(11)
95	10.15221(18)	6.98597(10)	9.98255(17)	100.801(1)	695.449(12)
85	10.14279(17)	6.98432(9)	9.97583(15)	100.738(1)	694.317(11)
75	10.13444(16)	6.98270(9)	9.97008(15)	100.681(1)	693.316(11)
65	10.12622(16)	6.98134(9)	9.96459(15)	100.630(1)	692.353(11)
55	10.11897(16)	6.98005(9)	9.95964(14)	100.580(1)	691.500(11)
45	10.11204(16)	6.97898(9)	9.95579(15)	100.535(1)	690.754(11)
35	10.10583(17)	6.97801(9)	9.95274(15)	100.501(1)	690.099(12)
30	10.10322(16)	6.97766(8)	9.95128(14)	100.482(1)	689.826(11)
25	10.10137(17)	6.97740(9)	9.95053(15)	100.476(1)	689.635(11)
20	10.09961(16)	6.97713(8)	9.94969(15)	100.462(1)	689.461(11)
15	10.09884(16)	6.97689(8)	9.94925(14)	100.460(1)	689.358(11)
10	10.09847(9)	6.97683(5)	9.94931(9)	100.458(1)	689.336(6)
Sample-2					
205	10.28024(4)	7.01445(3)	10.08060(4)	101.5836(4)	712.109(4)
200	10.27463(5)	7.01228(4)	10.07540(6)	101.5457(5)	711.230(4)
195	10.26877(7)	7.01007(6)	10.07013(7)	101.506(1)	710.328(6)
190	10.26233(8)	7.00873(6)	10.06519(8)	101.467(1)	709.496(7)
185	10.25614(9)	7.00632(7)	10.05989(9)	101.431(1)	708.543(8)
175	10.24134(5)	7.00289(4)	10.05166(6)	101.3497(5)	706.796(4)

Table S2, continued

T (K)	*a* (Å)	*b* (Å)	*c* (Å)	β (°)	V (Å^3)
Sample-3					
200	10.27354(9)	7.01277(7)	10.07592(10)	101.541(1)	711.253(8)
197.5	10.27140(26)	7.01229(20)	10.07467(26)	101.517(2)	711.029(21)
Sample-4 (first annealing)					
202.5	10.27640(10)	7.01350(8)	10.07805(10)	101.558(1)	711.632(9)
200	10.27340(11)	7.01270(8)	10.07556(11)	101.538(1)	711.218(9)
197.5	10.26966(9)	7.01189(7)	10.07292(9)	101.517(1)	710.743(8)
195	10.26709(15)	7.01038(12)	10.07048(14)	101.494(1)	710.297(12)
Sample-5					
200	10.27351(13)	7.01297(10)	10.07600(13)	101.541(1)	711.277(11)
195	10.2683(5)	7.0107(4)	10.0712(5)	101.493(5)	710.46(4)

Table S3

Parameters obtained by fitting of a second-order Debye model to the unit-cell parameters of DMSO-d_6·3D_2O between 10 and 195 K. The unit-cell edges, for dimensional reasons, are fitted as their cubes, but the 'derived' quantities present the results as linearized values.

	a^3	b^3	c^3	V
θ_D (K)	120(3)	110(7)	197(7)	139(3)
X_0 (cm^3 mol^{-1})	155.044(9)	51.129(2)	148.291(9)	103.786(3)
Q (x10^4 J cm^{-3})	183(3)	876(28)	200(7)	310(5)
b	5.5(3)	51(2)	5.0(7)	11.4(5)
		Derived parameters		
X_0 (Å, $Å^3$)	10.098(1)	6.9768(5)	9.950(1)	689.36(4)
K_0/γ	11.8(2)	171(5)	13.5(5)	29.9(5)
K_0'	12.1(5)	104(5)	11(1)	24(1)